International
Progress Report

IPR-09-12

Äspö Hard Rock Laboratory

The use of focused ion beams for structural characterisation of bentonite

A feasibility study

Marie Wegdén
Per Kristiansson
Division of Nuclear Physics, Lund Institute of Technology

Daniel Svensson
Anders Sjöland
Svensk Kärnbränslehantering AB

December 2007

Svensk Kärnbränslehantering AB
Swedish Nuclear Fuel
and Waste Management Co

Box 250, SE-101 24 Stockholm
Phone +46 8 459 84 00

Äspö Hard Rock
Laboratory

Report no.
IPR-09-12
No.
F136
Author
Marie Wegdén
Per Kristiansson
Daniel Svensson
Anders Sjöland
Date
December 2007
Checked by
Per Kristiansson
Date
2009-08-25
Approved
Anders Sjöland
Date
2009-09-09

Äspö Hard Rock Laboratory

The use of focused ion beams for structural characterisation of bentonite

A feasibility study

Marie Wegdén
Per Kristiansson
Division of Nuclear Physics, Lund Institute of Technology

Daniel Svensson
Anders Sjöland
Svensk Kärnbränslehantering AB

December 2007

Keywords: Ion beam analysis, STIM, PIXE, Bentonite, Buffer, Swelling, Structure, Porosity

Abstract

Bentonite clay is planned to be used in the KBS-3 concept for future nuclear high level waste (HLW) repository in Sweden. In the concept the spent nuclear fuel is placed in an iron insert, which is encapsulated in a copper canister. The copper canister is embedded in compacted bentonite and deposited at 500 m depth in granite bedrock. The compacted bentonite will act as a buffer material, giving mechanical support for the copper canister, reducing water movements and capturing potentially escaping radionuclides.

Bentonite contains high amounts of smectite minerals (most common is montmorillonite), which are swelling clay minerals. The smectite minerals are layered and have the ability to store water in its structure. This is done by intercalating water between the layers and expanding the interlayer distance. The exceptional swelling capacity makes bentonite a suitable buffer material that works as a sealant and barrier.

Heterogeneity in the material, compaction and in swelling may result in porosity, both on the nano- and micrometre scale. This may affect the permeability of the clay and may mediate the transport of radionuclides, cations and corrosion products.

The aim of this work is to investigate the feasibility of using common ion beam techniques for structural characterisation of bentonite, including studying the mineral composition and the coarse porosity. The analytical techniques used were scanning transmission ion microscopy (STIM), particle-induced X-ray emission (PIXE) and elastic p-p scattering, performed at the Lund Nuclear Microprobe. On-axis STIM analysis was performed in order to measure and map the areal mass density of the sample. Since it was impossible to differentiate an increase in thickness from an area of higher mass density, as well as discerning depth variations, the STIM analysis was also performed in tomographic mode, in an attempt to obtain 3D structural information. The tomographic reconstruction showed that the bentonite had an interesting internal structure, with micrometre-sized features indicating both accessory minerals and potential pores. PIXE analysis was performed subsequently for investigation and mapping of the element distribution in the samples. From these element maps, the different mineral phases and regions suitable for further analysis could be identified. Finally hydrogen analysis was performed with the elastic p-p scattering method, in order to measure the water content in the sample. This method can be useful in further examinations of bentonite, if the variation in porosity is to be studied as a function of the degree of water saturation.

This work demonstrates that, in a combination, PIXE, hydrogen analysis and microtomography with the STIM technique, can provide unique information on the internal structure and element distribution in a microscopic bentonite sample. Removal of water from the clay sample will change the clay structure and porosity due to the dehydration of the interlayer space and is hence problematic, however in this feasibility study this problem is neglected.

Sammanfattning

Bentonitlera planeras användas som buffertmaterial i KBS-3 konceptet, vilket är SKBs metod för framtida slutförvaring av använt kärnbränsle.

I metoden så kapslas det använda bränslet in i en kopparkapsel och placeras i kristallint berg på ca 500 meters djup. Mellan kapsel och berg placeras en buffert av kompakterad bentonitlera.

Buffertens syfte är att kemiskt och fysiskt skydda kopparkapseln under mycket lång tid. Leran är ett heterogent material som huvudsakligen består av svällande lermineral (smektiter) och då vanligtvis montmorillonit. De svällande lermineralen expanderar genom att ta upp vatten mellan kristallskikten. Förutom svällande lermineral finns bland annat kvarts, fältspat, glimmer, kristobalit, pyrit och kalcit som typiska accessoriska mineral.

Heterogeniteten i materialet eller från kompakteringen av leran kan eventuellt orsaka en mikroporositet i leran. Denna mikroporositet skulle potentiellt kunna påverka buffertens egenskaper.

Syftet med detta arbete är att undersöka möjligheten att använda jonstråletekniker för strukturell karaktärisering av bentonitlera med avseende på mineral sammansättning och grov porositet.

De analytiska tekniker som används är scanning transmission ion microscopy (STIM), particle-induced X-ray emission (PIXE) och elastic p-p scattering. Arbetet utfördes vid Lund Nuclear Microprobe.
On-axis STIM analyser utfördes för att mäta och kartlägga den rumsliga mass densitets fördelningen i provet. Då det inte var möjligt att skilja ett område med större tjocklek från ett med högre densitet, så utfördes STIM analysen även
i tomografi läge i ett försök att få ut tre dimensionell information. Den tomografiska rekonstruktionen indikerade att leran hade en intressant intern struktur med accessoriska mineral samt potentiella porer i mikrometer skala. PIXE analys utfördes för utvärdering och kartläggning av elementarfördelningen i provet. Från dessa kartor kunde individuella mineral faser identifieras. Väteanalys utfördes med elastic p-pscattering för att uppskatta mängden vatten i provet. Leran visade sig innehålla en mycket låg vattenhalt vilket indikerar att det låga trycket under mätningen torkat ut leran. Eftersom uttorkning gör att leran krymper så påverkas även strukturen och eventuell porositet av detta. Metoden kräver ett mycket litet prov och lågt tryck och detta ställer stora krav på provprepareringen om ett representativt prov ska kunna beredas. Eventuella framtida studier bör modifiera metoden för att förhindra uttorkning av leran.

Contents

1 Background

1.1 General

Bentonite clay is planned to be used in the KBS-3 [1] concept for future nuclear high level waste (HLW) repository in Sweden. In the concept the spent nuclear fuel is placed in an iron insert, which is encapsulated in a copper canister using friction stir welding (FSW). The copper canister is embedded in compacted bentonite and deposited at 500 m depth in granite bedrock. The compacted bentonite will act as a buffer material, giving mechanical support for the copper canister, reducing water movements and capturing potentially escaping radionuclides.

Bentonite is a natural clay, often described as an alteration product of volcanic ash [2] and has a high swelling capacity in water. The swelling properties of bentonite comes from the high content of smectite minerals, which are 2:1 phyllosilicates (layer silicates) clay minerals that can intercalate water into their structure while hydrating its interlayer cations and layer surfaces [3]. It is the exceptional swelling capacity that makes bentonite a suitable buffer material that works as a sealant and barrier [4].

Montmorillonite, which is the most common smectite mineral, consists of stacked negative layers with positive interlayer cations. Each layer consists of three sheets, the two outermost with tetrahedrally coordinated Si and Al, and the middle one with octahedrally coordinated Al and Mg. The layers typically have a thickness of 1 nm and a horizontal extension of several hundreds of nm [5]. The interlayer cations are exchangeable, and Na^{+} and Ca^{2+} are the most common. These interlayer cations compensate for the negative charge at the layer surface due to the solid solution substitution within the layers [6]. Hydration of interlayer cations will occur in discrete steps of up to four layers of water, with corresponding interlayer distances. This is called crystalline swelling [7]. At some conditions also osmotic swelling can occur, where the clay layers are fully dispersed and water is transported into the interlayer regions in the montmorillonite due to ion transport from high concentration to low concentration volumes. This leads to an increased interlayer distance.

The swelling will depend on the type of interlayer cation, layer charge and the salinity of the water. In a porous mineral structure, this swelling will reduce the pore volume until the original pore volume is filled with water, i.e. full water saturation [5]. Water can continue to move in order to balance the interlayer ion concentration in the system, and any remaining differences in ion concentrations lead to an osmotic pressure.

The final pore-size distribution determines the hydraulic permeability and governs the possible transport of colloids, and material transport by advective flow. Hence, also the thermal gradient around a copper canister of decaying fuel will contribute to a redistribution of water [8].

Heterogeneity in the material, compaction and in swelling may result in porosity, both on the nano- and micrometre scale, which may affect the permeability of the clay and may possibly mediate the transport of radionuclides, cations and corrosion products.

The aim of this work is to investigate the possibility and feasibility of using standard ion beam analytical techniques in the non-destructive study of the structure and coarse porosity in bentonite.

1.2 Common techniques

Common techniques for element analysis, coordination number identification and examination of the crystal structure of clays are scanning electron microscopy (SEM), X-ray diffraction (XRD), X-ray fluorescence (XRF), neutron activation analysis, X-ray absorption spectroscopy (XAS), nuclear magnetic resonance (NMR) and Mössbauer spectroscopy [8-11]. Reference [12] reports on investigations with gamma ray computed tomography of macroscopic porosity changes in soil due to repeated wetting and drying cycles. Several authors have reported on ion beam analysis of clays for element analysis, studies of uranium diffusion in bentonite [13] and cation exchange [14] with PIXE, RBS and PIGE. However, most analytical work has been performed in thick target mode or with broad beam [15]. Such conditions are not suitable for investigations of microscopic features such as pores or for the identification of single mineral grains, which is the main aim of this work. Therefore the complementary use of scanning transmission ion microscopy (STIM), particle-induced X-ray emission (PIXE) and elastic p-p scattering was applied to gain both structural and element information on the microscale. A STIM tomography experiment was also conducted in order to investigate whether three-dimensional mass density information, with sufficiently good spatial resolution to examine the micrometre-sized pore distribution, can be found.

2 Ion beam analysis

An ion can undergo a number of processes when it interacts with matter, for example, elastic and inelastic scattering with the nucleus or electrons in the material. It can also induce radiation by interacting with bound electrons or cause emission of secondary electrons or ions. Ion beam analysis is performed by detecting the energy distribution of the emitted particles or radiation, either of which can be useful in characterizing a specimen and can provide information about elements, isotopes or chemistry. Ion beam analysis refers to several analytical techniques, among others, PIXE, RBS, ERDA and NRA [16].

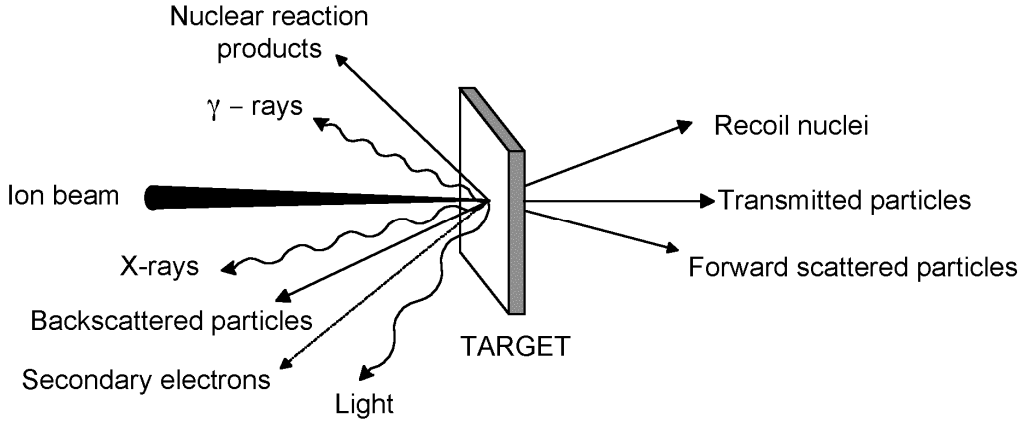

Figure 2.1. *Various processes that can occur when an MeV ion beam interacts with matter.*

A focused ion beam from an accelerator can be used to extract information of microscopic scale from a sample. Combined with other instrumentation (detectors, data acquisition system etc.) it can be used as a micro analytical tool: a *nuclear microprobe* (NMP). The instrument can be used to determine concentrations of elements with high sensitivity. Coupled with a scanning system, two-dimensional "depth-average" distribution information can be generated with a lateral resolution of a few micrometers or less.

The benefit of ions at MeV energies, e.g. in comparison with electrons, is that they penetrate deeply (a few tens of micrometers) without marked scattering, and consequently retain the beam spot resolution to a significant depth [17]. Most of the individual particles penetrate the specimen and roughly retain their incident direction. Only a small proportion of the particles will come sufficiently close to the nucleus of an atom in the specimen to scatter or cause nuclear reactions and be lost from the beam.

2.1 Analytical techniques

The analytical techniques available for a nuclear microprobe can be divided into two classes: high beam-current techniques and low beam-current/single ion techniques. The low beam-current techniques, e.g. STIM (Scanning transmission ion microscopy), can generate images with better spatial resolution, but the high-beam current techniques, e.g. PIXE (Particle-induced X-ray emission, NRA (Nuclear reaction analysis), RBS (Rutherford backscattering spectrometry) and ERDA (Elastic recoil detection analysis) are better for analytical purposes.

A brief introduction on the standard techniques used for the bentonite analysis in this work is presented in the following paragraphs. More extensive information on ion beam methods can be found in reference [18-20]. A more detailed description on practical and experimental aspects on the methods are presented in chapters 3 and 5 in this report.

2.1.1 Particle-induced X-ray emission (PIXE)

Particle-induced X-ray emission is based on the excitation of electrons from the inner shells of the atom, induced by a colliding charged particle, e.g. protons or alpha particles. Outer shell electrons recombine with the vacancy, and result in X-ray emission at an energy characteristic of the atom under bombardment. PIXE is a multi-element method (see figure 2.2) with a practical use for all elements heavier than manganese or aluminium. Characteristic X-ray energies for elements with lower atomic numbers (<Al) are so small that they are absorbed in the detector window [18], but to cover also elements in the lower part of the periodic table, PIXE is often supplemented by other techniques that can provide complementary information on the specimen.

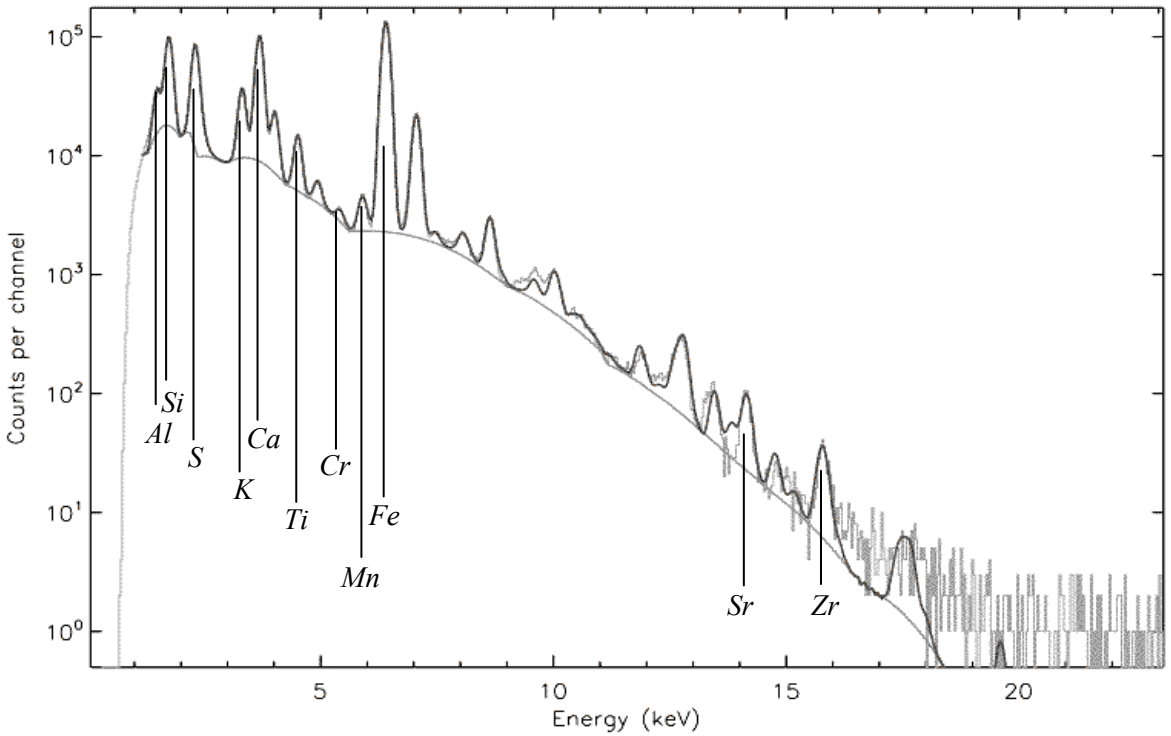

Figure 2.2. *Typical multi-element PIXE spectrum from an aerosol sample. Some peaks are marked with their potentially corresponding element, in order to schematically illustrate the principle for element identification.*

PIXE analysis is fast, essentially non-destructive and the low background facilitates trace element analysis in small samples. With a spatial resolution of a few micrometres, absolute detection limits of the order of 10^{-15} – 10^{-16} g can be obtained for thin samples [19]. The detection limit, however, depends on several factors, such as the target element, the sample matrix and the energy of the projectile. Therefore the detection limit has to be separately evaluated for every sample and element.

2.1.2 Elastic recoil detection analysis (ERDA)

In ERDA the energy of the recoiling target nucleus is measured. The kinematics allows the recoil to occur only in the forward hemisphere and the projectile, which is often incident at a glancing angle, should have a higher mass than the target nucleus. ERDA complements Rutherford backscattering spectrometry in measuring light elements in matrices of medium or high average atomic number. An absorber foil in front of the detector stops scattered beam particles and allows only ejected particles to reach the detector, at the price of degrading the depth resolution. High-resolution ERD systems with electrostatic deflectors for blocking scattered beam particles overcome this problem, and depth resolutions of 0.28 nm have been reported [21].

The hydrogen method described in section 2.2 is a special case of ERDA with equal mass of projectile and recoiling target nucleus.

2.1.3 Scanning transmission ion microscopy (STIM)

The method is based on the measurement of the energy loss of beam particles travelling through the sample. The energy loss is caused by ion-electron interactions and the magnitude of the total energy loss depends on the elemental concentration, mass density and thickness of the sample.

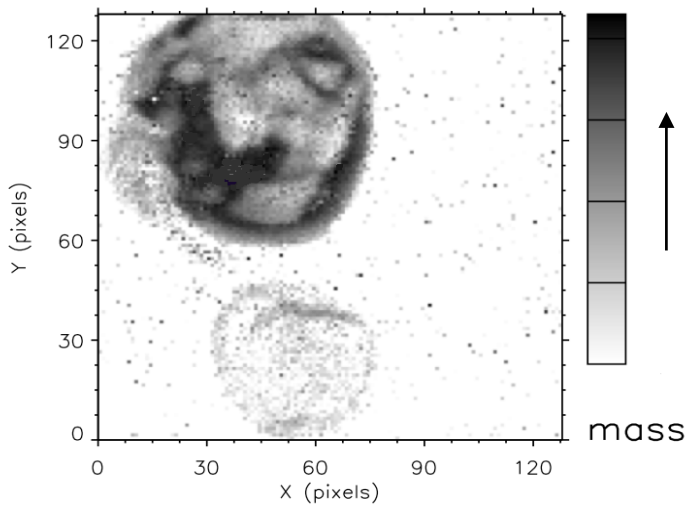

Figure 2.3. *STIM map of fungi spores. Notice the internal structure in the upper spore. Pixel size: 1 μm.*

On-axis STIM provides high spectral resolution, and requires the detection of only a few transmitted particles. This is advantageous for samples that are sensitive to mass loss when higher beam intensities are used. Another option is to position the detector at some suitable angle, a setup called off-axis STIM. Since the angle between the beam and the detector is small (10–15°) the information is about the same as with on-axis STIM. Off-axis geometry makes it possible to use analytical beam-currents and STIM analysis can thus be performed simultaneously with for example PIXE or RBS, but spectral degradation will decrease the contrast compared to the on-axis case. The particles can also reach the detector by scattering in a thin carbon foil placed behind the

sample (on-axis/off-axis STIM). The geometry is then sensitive only to pure energy loss, and ions scattered in the sample will not influence the spectral shape because they are off-collimated [22]. Figure 2.3 shows a STIM map of fungi spores with visible internal structures.

2.2 The Lund Nuclear Microprobe laboratory

The Lund Nuclear Microprobe laboratory is based around a single-ended electrostatic 3 MV Pelletron accelerator (model NEC 3 UDH). Inside the pressure tank is a radio-frequency ion source, which can produce protons, alpha particles and occasionally also deuterons from hydrogen, helium and deuterium gas. The pressure tank is filled with insulating gas, SF_6, to prevent sparking.

Charge is inductively sprayed onto the pellet chain and picked off at the high voltage terminal to create a potential difference between the HV terminal and ground at the exit side of the accelerator. The ions from the ion source are then accelerated towards ground, attaining a maximum energy of 3 MeV per unit charge. The analysing magnet serves as a momentum filter where ions of the correct charge and velocity are selected to pass into one of two beamlines: *macro and sub-micron*, each leading to a separate experimental chamber via a beam optimisation system. Along the beamlines vacuum pumps are strategically positioned to maintain high vacuum along the beamline and in the experiment chamber. The experimental work described in this report has exclusively been conducted at the sub-micron beamline.

Magnetic quadrupole lenses are used to focus the MeV ions. Since a quadrupole magnet focuses in one plane and diverges the particle beam in the other, at least two quadrupoles of opposite polarity are needed to focus an ion beam [18]. The demagnifiacation of the ion beam onto the target is set by a combination of the size of the object collimator, the distance from the object slit package to the target and the properties of the focusing magnets. The shaping and elimination of divergent parts of the beam are performed with the aperture slits. Different combinations of object and aperture slit size, together with the excitation of the quadrupole magnets, control the beam size and current conditions. The three beamlines are schematically shown in figure 2.4.

The first beamline, the macro beamline, is situated at +30° from the exit port of the accelerator and utilizes a quadrupole doublet to produce an enlarged homogeneous beam (1-10 mm) in the chamber, with a typical current between 1 and 200 nA [23,24]. This beamline is used mainly for quantitative PIXE analysis of for example aerosol samples.

The second and most recently installed beamline, replacing the old micro beamline is the sub-micron beamline, situated at -15°. It has a two-stage focusing system consisting of two separated doublets, where the beam is focused to a small spot in the first stage, which is then used as object in the second stage in which the ion beam is demagnified again to sub-micrometre dimensions [23]. Theoretical calculations on beam optics show that a beam spot of 200 nm × 500 nm is attainable with this setup [25]. The beamline was mechanically ready late in 2003 and since then the work on further development, installations in the experiment chamber, as well as testing and optimisation of the beam optics has continued.

Since a reduction of the beam spot is made at the expense of beam current, an annular, large-area HPGe-detector (8×100 mm^2) has been installed for traditional PIXE analysis [25]. The large and flexible experiment chamber can accomodate other detectors, such as surface barrier detectors in the forward or backward direction for NRA, RBS or other scattering experiments. Small detectors can easily be mounted on the movable stage for chamber microscope objectives. The chamber is equipped with a movable X-Y-Z sample stage controlled by step motors with nm precision. For tomography experiments, the sample holder can be replaced by a rotation motor (DC-Motor-Gearhead C136-10 drive unit), which is capable of high precision rotation in steps of 0.0068° at an approximate speed of 1200°/s.

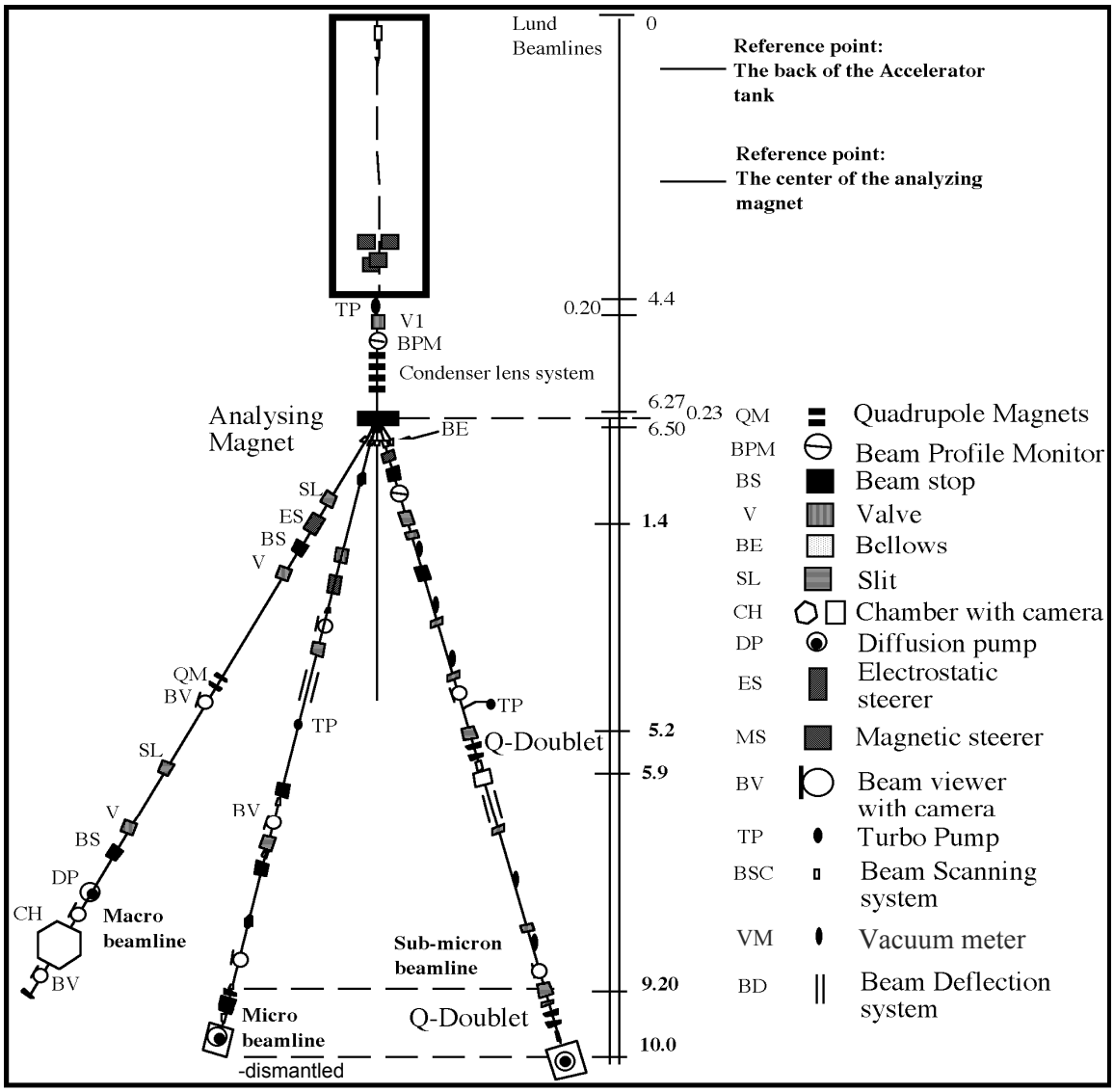

Figure 2.4. *Schematic diagram of the three beamlines at the Lund Nuclear Microprobe.*

The micro and sub-micron beamlines are equipped with post-lens magnetic scanning systems, which are used for rastering the beam over a large sample area to obtain two-dimensional information on the elements in the sample. Both the micro and the sub-micron beamline have fast beam blanking systems, for instance for proton beam lithography experiments, when the beam needs to be blanked during movement between pattern pixels or to control beam exposure times. The electrostatic blanker plates are controlled by a TTL signal that is fed to a high voltage amplifier and the beam is deflected off the sample within 200 ns [26].

All three experiment chambers allow charge measurement in Faraday cups in transmission geometry or from the sample via the sample holder. An important improvement at the sub-micron beamline is that the beam blanker is combined with a pre-target Faraday cup for accurate and sample-independent charge measurement [27]. The beam is blanked into the pre-target Faraday cup at some point during the exposure of the sample. How often, and for how long the charge is measured depends on how much beam time the experimentalist is prepared to sacrifice. Typically it is reasonable to sacrifice 10-20% of beam time in high-precision charge measurements. The readout of the Faraday cup is made either by connecting it to a charge integrator or to a Keithley 6514, low-current electrometer. The charge integrator has a sensitivity level of 100 pulses/pC, but has a recovery time of 0.5 s, which makes pixel-by-pixel charge or current measurement impossible at standard scanning frequencies. The Keithley electrometer can measure currents in the fA region, but with long integration times (typically 2.5 s). Therefore this instrument is useful only for measurements for low beam-current control and adjustment, not for charge or current measurements under data acquisition conditions. With the pre-target Faraday cup, the flexibility of the charge measurement system is maintained, and it can be used for a wide range of beam current conditions.

3 Analytical methods

The aim of the analysis was to investigate the composition and structure of bentonite clay at micrometre resolution. The analytical methods should be non-destructive and for the examination of the porosity in bentonite, the three-dimensional pore-size distribution should be revealed. If the analysis proved to be promising, further studies of series of samples can be performed to measure the effect of water content on the porosity. For this reason, hydrogen determination was also included as a part of the study in order to examine what water concentrations can be expected.

The STIM method was chosen to measure the mass distribution in thin, bentonite films, prepared according to the drying procedure presented in chapter 4. If the standard 2-dimensional technique showed not to be successful, the STIM examination would be expanded to involve a tomography experiment.

For mineral identification, PIXE analysis was chosen. Via the element distribution information, mineral phases can be identified and correlated to the mass density maps from the STIM analysis.

In the following paragraphs, the methods for hydrogen analysis and STIM tomography will be described in more detail. Both methods are special variants of standard methods that are used more commonly in ion beam analysis. The description concerns the physics behind the method as well as experimental and analytical issues.

3.1 Hydrogen analysis with ppm-sensitivity

Hydrogen is the most abundant element and is one of the main constituents in water and organic material. It is also the most common elemental contaminant and its presence can have dramatic effects on the electrical, mechanical and chemical properties of materials. Having a valence of both +1 and -1, it is chemically versatile and can react with most elements. Hydrogen is also by many orders more mobile than other common contaminants, even at room temperature. [18]

Many research disciplines such as geology, materials science, biology and medicine have a strong interest in quantitative and spatially resolved data on the hydrogen distribution in a sample. Every application has its own special needs, either concerning radiation- sensitive samples, low hydrogen concentrations, demands on resolution etc., and the analytical method to provide answers to the specific questions, must be adapted to fit the special requirements. Most common analytical techniques, such as PIXE, RBS, Auger electron spectroscopy etc. cannot detect hydrogen. Variations on ERDA and NRA are widely used, but are considered to be restricted to surface analysis or require projectile species and/or energies, which are not available at the Lund Nuclear Microprobe facility.

3.1.1 Elastic proton-proton scattering

The proton-proton scattering technique was introduced by Cohen et al. in 1972 [28], and requires transmission geometry (see figure 3.1) and that both the recoiled and the scattered particle are detected. Therefore only thin samples can be analysed. Elastic proton-proton (p-p) scattering deals with equal masses of projectile and target nucleus, which at non-relativistic energies has the result in that the sum of the scattering and recoil angles is exactly 90° in the laboratory system. Scattering on hydrogen nuclei (i.e. protons) can therefore be distinguished with high precision from scattering on other elements in the sample if the detectors are positioned wisely.

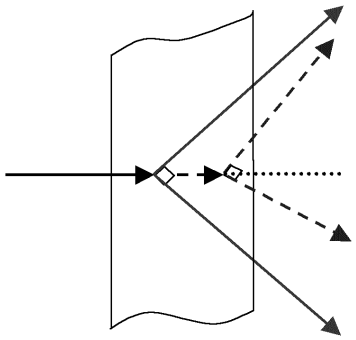

Figure 3.1. *Illustration of the p-p scattering geometry.*

One alternative is to position two detectors in 45° to the direction of the incident beam, as described by Cohen et al. in their revolutionary paper. However, the detectors must be small, in order not to accept too large an angle interval around 45°. This is not good in combination with the wish for a large solid angle to reduce the radiation damage to the sample. The use of larger detectors, by which the transmitted particles are detected in coincidence, in combination with a scattering and recoil angle identification process, is then a more attractive alternative. Both methods are capable of depth profiling if the residual energy is measured. The major advantage of the latter method lies in the possibility to use large solid angle detectors without sacrificing depth resolution.

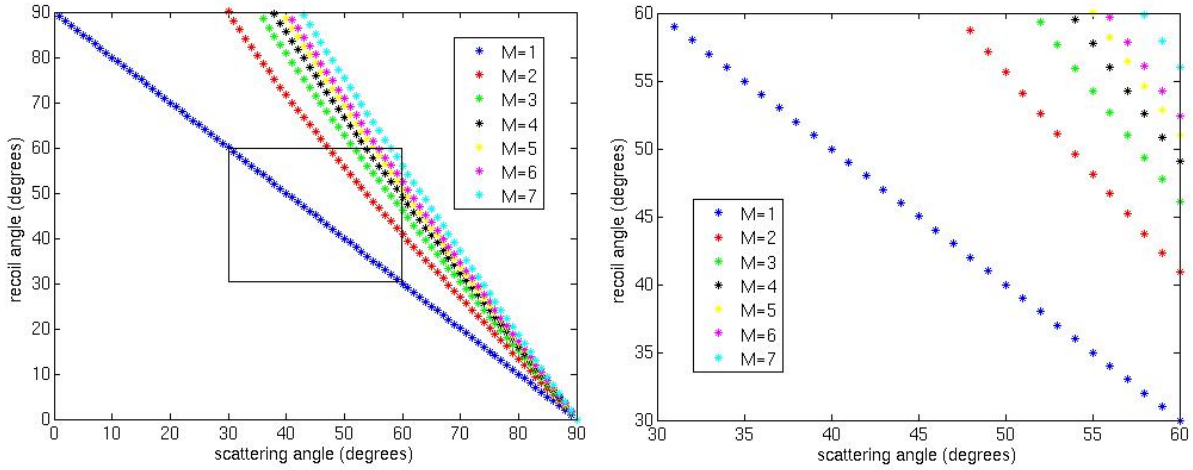

Figure 3.2. *The resulting recoil angle for a target of mass number M when bombarded with protons (M=1) scattered into the forward hemisphere. Figure (b) is a close-up of the boxed region in figure (a) and corresponds to the angle coverage of the hydrogen detector used in the experiments.*

Figure 3.2 shows, the angle coverage that would be desirable, in order to avoid signals from disturbing elements, and at the same time maintain an acceptable solid angle. Calculations of recoil angles for elastic scattering on different elements with a proton beam as projectile and scattering angles in the forward hemisphere, show that, with the strict constraint of 90° between scattered and recoiled particle, there is no possibility for

simultaneous detection for any other target than hydrogen in the 30-60° interval. This angle interval is chosen symmetrically around 45° with the intention to maximise the solid angle and avoid all interference due to elastic scattering with other elements. No overlapping angles whatsoever can be observed in this safe region, and restricting the angle interval even further makes accidental detection caused by multiple scattering impossible. Transmitted particles do not constitute a problem because of their nearly linear propagation in matter. It is not very likely that multiple scattering causes a deviation of the proton direction by as much as 30° and, in combination with a strict coincidence condition, such events are efficiently eliminated. The coincidence condition also deals with inelastic scattering events and particles from nuclear reactions with energies lower than the incident particle. The "one-element specificity" eliminates the problem of background subtraction, which enhances the sensitivity [29].

Hydrogen analysis with the p-p scattering method offers:

- High sensitivity (ppm-level)
- Minimum beam damage effect compared to other similar methods
- Depth profiling with micrometre resolution

The depth profiling ability of the method allows reliable measurements on bulk concentrations of hydrogen, away from the ever present surface contamination peak (as illustrated in figure 3.3).

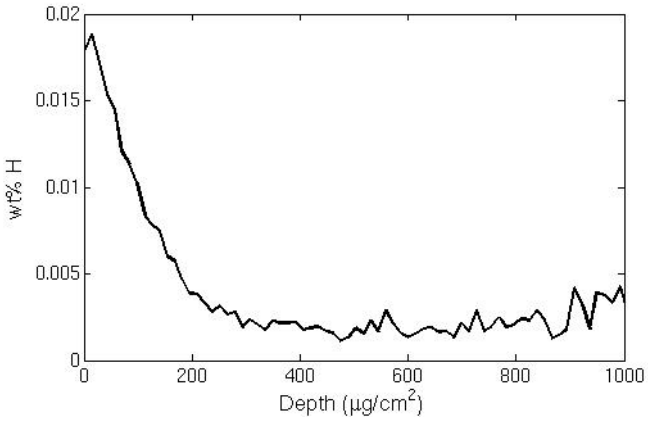

Figure 3.3. *Hydrogen depth profile of orthopyroxene with a distinct surface contamination peak.*

Over the years, the p-p scattering method has not been widely used as an analytical technique. The method is less conventional than the standard ERDA technique, which does not offer as good damage number or analytical depth as the p-p scattering method, but, on the other hand, it does not require the same sample preparation technique where the samples are thinned down to allow particle transmission. More recently however, the possibility of using the p-p scattering method in microprobe applications has attracted interest, and is now being applied at microprobe laboratories in Sweden, Germany, France and Japan, both at low and high energies. In Lund, proton-proton scattering experiments have been performed in several application areas, such as in aerosol science and in depth profiling of nominally anhydrous minerals with ppm levels of H as a complementary method to FTIR. [30-34].

3.2 Tomography with focused ion beams at MeV energies

The word *"tomography"* originates from Greek, with the meaning tomo – slice or cut, and graphy – write. An image of a slice, or a cross section, of the object can be derived mathematically, by illuminating the object from many different angles and measuring how the radiation is affected by passage through the object, either in terms of intensity or energy loss. By combining a set of projections, commonly acquired at intervals through 180 or 360 degrees around the object, a *reconstruction* of the object can be produced by applying different mathematical algorithms. By stacking many of these reconstructed cross sections on top of each other, a full three-dimensional image of the object can be produced.

Today, tomography is used in many diverse research areas and in industry to perform non-destructive examinations and gain cross sectional or true three-dimensional information on test objects. Not only X-rays are used for the imaging, but also other kinds of electromagnetic waves or particle radiation. The impressive range in object size stretches from proteins imaged by NMR/MRI to investigations of the interior of the Earth by seismic tomography.

The traditional, two-dimensional mapping with ion microprobes, was extended to tomographical investigations in the mid 1980's, independently by several research groups [35,36]. Two main types have been developed, STIM and PIXE tomography, in which the mass density and element distribution, respectively, are imaged. The mass density maps are useful to image the morphology in the sample and reveal internal structures or pores. Three-dimensional mass density information can then help to perform a more correct mass density normalisation for PIXE experiments, where the usual assumption of a homogeneous element distribution over the whole sample thickness might be erroneous. To take things one step further, subsequent PIXE tomography can be performed to reach real, three-dimensional element distribution imaging and thus avoid depth-averaged quantitative data.

Ions interact differently with matter than for instance X-rays, and experience both energy loss and scattering when traversing matter. This limits the range for MeV ions, often to 10-100 micrometres, depending on the initial energy, the ion mass and the target material. The range sets a limit on the maximum specimen thickness that can be analysed in transmission mode, or the maximum analytical depth of analysis in emission mode. On the other hand, the possibility to focus ion beams to micrometre and sub-micrometre size, as well as the small lateral straggling as compared to e.g. electron beams, makes them well suited for high-resolution analysis of microscopic samples such as cells, spores etc.

Tomographic investigations are time-consuming and require very small sample dimensions, and have therefore not replaced standard, two-dimensional mapping, which delivers sufficient information in most applications. For specific questions at issue however, tomography can be a source of valuable information, which simplifies the interpretation of data and makes features visible, which cannot be distinguished in only two dimensions.

3.2.1 Reconstruction techniques

The basic idea of image reconstruction is to convert the projection data, the sinogram, into an image. There is a large variety of reconstruction techniques, which can be categorised into three basic groups: *algebraic, analytical* and *statistical methods*. Also there are iterative versions of these techniques. The choice of reconstruction technique is based on the speed of the algorithm, how artefacts influence the image quality and the possibility to introduce corrections during the reconstruction to take into account different physical phenomena, such as X-ray attenuation in the case of PIXE tomography.

The mathematical solution to the reconstruction problem was completed by Radon in 1917. The method of backprojection was used in the first CT-scanner, and was later also commonly used in radioisotope emission methods. Also today, the more advanced version, filtered backprojection, is one of the most commonly used reconstruction techniques, at least in medical tomography. It is known to be fast, maybe the fastest, and accurate.

3.2.2 STIM tomography

In STIM tomography, the energy loss of transmitted particles is measured and transformed into areal mass density values for every projection. The reconstruction process will result in an image of the mass density distribution (in g/cm^3) in a cross section of the sample. STIM-tomography is executed with on-axis geometry to optimise the energy resolution, and the energy and ion species is adjusted for optimal contrast in the object in question. A typical experimental setup is illustrated in figure 3.4.

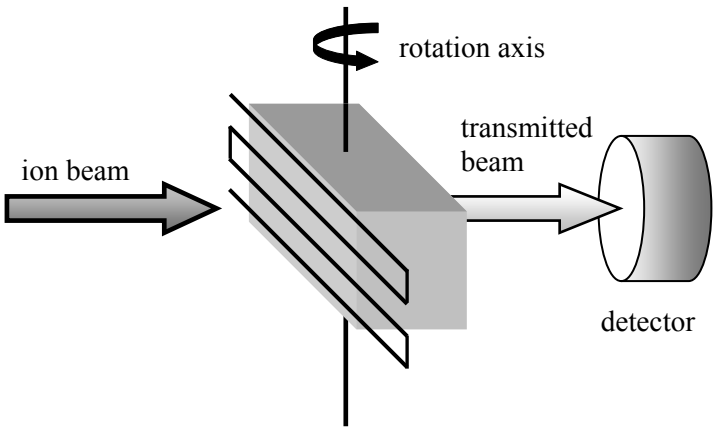

Figure 3.4. *Illustration of the geometry for STIM tomography.*

In every ion beam experiment it is important to deliver as small a dose as possible to the specimen, to avoid shrinking effects due to heating, redistribution of volatile elements etc. Here STIM tomography is a suitable candidate for fragile samples since, despite the long irradiation times required, the current conditions in place guarantee minimum sample damage.

3.2.3 The Lund tomography system

For tomography experiments, the ordinary sample holder is replaced by a sample manipulator attached to a "DC-Motor-Gearhead" drive-unit (Model C136-10 from Physik Instrumente (PI)). The manipulator is attached to a stage, which can be manually tilted by adjusting a ball pivot, and this stage is mounted on the standard X-Y-Z sample stage. A tungsten needle with a 0.6 μm radius at its tip is used as the rotation axis and the rotation motor is capable of rotation in steps of 0.0068°. The manipulation of the rotation axis is controlled by the data acquisition system. The stage, on which the sample manipulator is mounted, also holds a rod with a calibration grid attached to a quartz plate (see figure 3.5). This assembly is utilised for focusing the beam and for determining the size of the beam spot.

The STIM detector is a windowless Hamamatsu p-i-n diode (S1223, 4×4 mm), which is mounted in on-axis geometry on the moveable stage for the rear microscope in the experiment chamber. This allows for small movements in the X-direction in the detector position, to avoid local detector damage during the experiment.

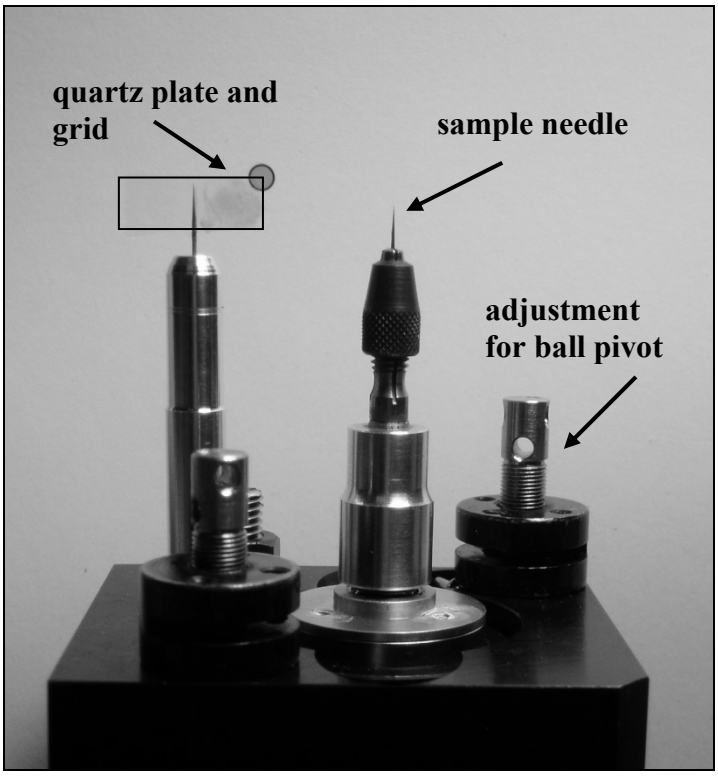

Figure 3.5. *Setup for sample manipulation including a copper grid and a quartz plate for beam focusing.*

The alignment of the rotation axis has to be performed in air. The sample is viewed in the rear microscope as it is rotated, and the pitch screws for the ball pivot are adjusted until the sample rotates nicely around a vertical axis. Unfortunately, no matter how good it looks in air, the alignment is subject to changes when the chamber is closed and pumped for vacuum.

4 Sample preparation

The sample preparation technique is a non-trivial problem, since the ion beam analysis requires thin samples that are not damaged by the environment in the vacuum chamber. This excludes the introduction of liquid water in the samples. Water removal can be performed with standard cryo-preparation methods [8], but ordinary drying is sufficient if the possibility that elements can undergo redistribution is taken into account. Removal of water from the clay will change the clay structure and is hence problematic, however in this feasibility study this problem is neglected, and any further studies should also improve the sample preparation technique.

The ion beam examination of the bentonite requires thin samples, of the order of some tens of micrometres. For PIXE analysis, the standard of thick geometry for geological samples may be sufficient, but both STIM and hydrogen analyses require transmission geometry and thus thin samples. The range of protons in bentonite is estimated to be 70 micrometres for 2.5 MeV protons from SRIM simulations [37]. For hydrogen analysis, a maximum thickness of 20 micrometres is reasonable to be able to gather some depth profile information and still allow transmission of both scattered and recoiled protons. The effect of beam straggling was also evaluated with SRIM simulations. A 2.55 MeV proton beam passing through a benonite matrix of 12 μm respective 18 μm thickness, experiences a lateral straggling of 0.16 μm respective 0.36 μm (FWHM). With a typical beam spot size of approximately 1 μm, beam straggling is not considered to seriously deteriorate the spatial resolution.

The clay material is brittle, and therefore sectioning to the required thickness is not trivial. If baked into epoxy, the clay can be cut with a microtome or ground and polished down to the appropriate thickness, but this implies the risk of contamination and or change in the natural porosity as the epoxy penetrates into the clay.

For the tomography experiment, the ideal sample would be bentonite clay enclosed in a microcapillary. In this way, the sample would be enclosed in a well-defined vessel, which makes the tomographic reconstruction much easier. However, a sufficiently thin capillary with a suitable wall thickness and inner diameter has not been found commercially. Moreover, the additional stopping in the glass, which further limits the dimensions of the sample itself is a potential drawback. Also, glass is very similar to any geological material, which could be another disadvantage. Introducing clay into a capillary also demands that the mineral fragments in the clay slurry are sufficiently small to be able to enter the capillary. In such a grinding procedure preservation of the original porosity is not possible, and there is a risk that the fragments are adsorbed in a size-dependent way on the walls of the capillary.

Finally, a simple procedure based on slurrying the clay with water and letting it dry was chosen for the preparation of the sample. The bentonite was of Wyoming type, MX80, from the American Colloid Company, and had been dried and milled to mm-sized grains. It typically consists of 80% montmorillonite, with sodium as the predominant interlayer ion, and 20% accessory minerals such as feldspars, quartz, calcite and pyrite [5]. 20 mg of bentonite was dipersed in 1 ml of milliQ water, and was then decanted to avoid large grains. The clay gel was injected into a mould made of a sample holder ring glued to a Mylar foil. After drying at room temperature for 24 – 48 hours, the Mylar foil

was removed, leaving a thin self-supporting film on the sample holder ring. If made even thinner, the clay film is very brittle and can, with advantage, remain on the supporting Mylar foil. The plate morphology of montmorillonite resulted in a clay film that was highly oriented along the c-axis. However, the representativity of these dried bentonite films as compared to unaffected clay can be questioned and in future studies other sample preparation methods must be developed.

For the tomography experiment a thin strip is cut from a dried clay film, having dimensions suitable for the transmission of ions in all directions. This strip is carefully attached to the needle on the rotation axis with carbon glue.

5 Experimental procedure

The sample analysis was performed in three subsequent steps; first STIM analysis, followed by PIXE analysis and finally hydrogen analysis. The three analytical techniques were not applied simultaneously, since different optimal experimental conditions, such as the analytical beam current, were required. In the tomography experiment only STIM analysis was performed since hydrogen analysis was prevented by the dimensions of the rotation motor and by the fact that the hydrogen detector could not be positioned as closely to the sample as needed. On-axis STIM was chosen for its unsurpassed contrast, as compared to the off-axis variant. Also, the data acquisition system could only handle eight ADC signals simultaneously, and it was desired to use as many elements as possible of the large-area HPGe detector [25] to shorten the analysis time or improve the statistics in the PIXE analysis.

For all experiments, 2.55 MeV protons were used, with beam currents of 100-300 pA for the hydrogen and PIXE analysis. No filter was used on the PIXE detector, since we wanted to map all visible elements in the sample. A unit step size of 0.6 micrometres was used for the STIM measurements, with a beam size of 1.5 micrometres and a maximum count rate of 10 kHz. Bentonite films of different thickness, both self-supportive free films and films with remaining Mylar backing were analysed. For standard STIM and PIXE examination, several areas were analysed with varying step size (multiples of the unit step size) in the maps. Both central areas and near edge regions were analysed. Regions aimed for analysis with complementary methods, the region of interest was chosen close to a sample edge or another characteristic feature, to assure that the same region could be identified and analysed with the subsequent methods if simultaneous analysis was not possible.

5.1 On-axis STIM analysis

The ion beam is focused according to standard procedures, after which the beam current is decreased towards STIM conditions by closing the object slit step-by-step. The STIM detector is positioned slightly off-axis, in order not to damage it by beam-currents which are too high. The detector is slowly moved closer to its on-axis position, while the object opening is further decreased so that the detector count rate from a calibration sample remains below 10 kHz. The on-axis position is confirmed by letting the beam pass a hole in the calibration sample. When the beam is off-axis, ions reach the detector via scattering in the calibration sample, but no scattering can occur in a region with a hole. In the on-axis position, straight propagating ions can reach the detector, without relying on scattering in a sample, and hence the incident ion energy can be measured with the detector. Energy calibration is performed with calibration samples in combination with tabulated stopping power information for the material.

A number of ions are detected in every pixel as the beam is scanned over the sample. To present the residual energy in a two-dimensional map, the average or median energy value of the ions detected in every pixel is calculated. Both methods are advantageous in different situations. Taking the median value requires fewer detected ions per pixel for a representative value than with average value filtering, and offers sharp resolution

as well as lower noise levels [38-41]. Average filtering is, on the other hand, generally better in resolving small structures, even with sub-beam resolution for features of highly varying density [42], which is important in the search for micrometer-sized pores, why exclusively this kind of filtering has been utilised in this work.

Energies that apparently do not originate from a transmitted ion, and hence would strongly impair the average value, are eliminated by introducing an energy window in the energy spectrum, into which a detected ion has to fit in order to be accepted. Examples of false events that can reach the detector, but can be eliminated with the energy window, originate from slit scattering, pulse pile up etc [43].

5.2 STIM tomography

A set of STIM maps with projection data from the sample are collected, covering 0-180 degrees. Each projection was acquired with a count rate of less than 10,000 ions per second and a scanning frequency of 250-1000 Hz. The image was scanned twice if zero-pixels appeared in the image. The scan region was selected to cover the tip of the sample, to always have a reference point in the image whose y-position should be constant in the case of perfect precession around a vertically aligned rotation axis. Small deviations from the ideal rotation may be corrected for off-line with dedicated software. Ideally, the sample should be mounted on top of the needle, symmetrically on the rotation axis, but since this is very difficult to achieve with the crude sample mounting technique described earlier, the sample often ends up glued flat to one of the sides of the tip of the needle. To save time and avoid scanning over the majority of zero-value pixels outside the sample, the scan region is selected reasonably tightly around the sample, and is allowed to follow the sample as it rotates.

As a rule of thumb, one ray should be utilised per resolution element and the ideal number of projections is $(\pi/2)N_p$, where N_p is the number of horizontal pixels in a projection. [43,44] A typical count rate of less than 10 kHz and a scanning frequency of 250 Hz, gives up to 40 detected protons per pixel, which is a more than sufficient number to get a well-representative value of the average residual energy for every pixel. The data acquisition at every projection angle, however, turned out to be very time demanding, and only 46 projections were made during an irradiation time of several hours.

5.2.1 Data analysis and reconstruction

The projection data were stored both as event files for later processing and as two-dimensional STIM maps. The STIM maps display the energy difference between a preset maximum energy, typically the incident ion energy, and the average residual energy in every pixel. All projection data are tagged with the corresponding rotation angle. The STIM maps were converted to areal mass density maps with the use of the mass densities that are known from the calibration sample, or by the use of stopping power data for a known sample composition assuming that the sample is homogeneous. The standard filtered backprojection algorithm was chosen for the reconstruction [45], since it is known to be fast, easy to implement and able to produce images of good quality. The algorithm is realised in MatLab, using predefined functions (e.g. “iradon”) from the image processing toolbox for the purpose. Before applying the filtered backprojection algorithm, data are corrected and adjusted with an in-house- written

computer code for improper alignment, for identifying and adjusting the rotation axis and for identifying zero-pixels. The principle for adjusting the rotation axis has been described by Azevedo et al. [46]. The inverse Radon transform is implemented for every horizontal line in the projection data set, with a free choice of filter, interpolation method and frequency cut-off. The filter is designed directly in the frequency domain, and the projections are zero-padded before filtering to prevent spatial domain aliasing and to speed up the fast Fourier transform [47].

In order to maintain as much information in the image as possible, and avoid deterioration of the resolution by smoothening processes, very little image processing was performed. No frequency cut-off was applied in the filtered backprojection process. If the reconstructions for each horizontal line in the projection data set are stacked, the full three-dimensional information is gathered and can be displayed in different ways. The sample morphology can be illustrated by selecting a mass density value to produce an iso-surface, or equidistant cross sections can be presented. A cut can be realised at any position in the sample to reveal the internal structure. With special volume-rendering software, outer contours and layers of the sample can be made transparent to mediate the visualisation of internal structures of a defined mass density. This is illustrated in chapter 6.4.

5.3 Hydrogen analysis

The hydrogen analysis was performed with a beam current of 100 pA and a beam size of approximately 5 micrometres. A surface barrier detector, divided into two halves, covering a total solid angle of 1.5 sr and accepting angles between 30 and 60 degrees was used for the particle detection. The coincidence between signals in the two detector halves was used as the gate for the experiment, and off-line filtering involving requirements on energy (a hydrogen event leads to a characteristic angle of 90 degrees between scattered and recoiled particle) and more narrow coincidence time, made it possible to achieve an almost background-free hydrogen quantification. Mylar foils with a known hydrogen concentration of 4.1 wt. % were used as standards.

6 Results and discussion

6.1 STIM analysis

The sample preparation technique resulted in adequately thin samples for all types of analysis in transmission mode. However, it was concluded that the measured thickness was less than expected, maybe due to more pronounced drying than expected and/or inhomogeneous drying on the Mylar foil. Both free, self-supporting samples that had been removed from the Mylar backing and Mylar supported samples were analysed. Figure 6.1 shows the STIM image of bentonite on 2 µm of Mylar (0.28 mg/cm^2), with scan sizes of (a) 1200×1200 µm^2, (b) 300×300 µm^2 and (c) 75×75. The lower left area of figure 6.1 (a) is zoomed in figure (b), and the same procedure is conducted between figure (b) and (c). The colourbars present surface density data in mg/cm^2. Hence, darker areas illustrate areas with higher areal mass thickness. However it is only possible to determine if an increase in mass thickness is due to variations in sample thickness or higher volume density if the element distribution is known.

In figure 6.1 (a), a crack or wrinkle is visible. This could be a wrinkle in the backing material causing an inhomogeneous drying of the bentonite slurry in that region. After subtraction of the mass of the backing foil, no empty pores can be identified in any of the figures (a)-(c) with certainty. A pattern is distinguished in figure (c), with small regions of lower mass density (three such regions are circled in red). This can indicate micrometre-sized pores, which are embedded in the sample at some thickness, but these regions could also represent inhomogenieties in the sample thickness or the element distribution. Nothing can be concluded with certainty. The high mass density regions (black spots) are identified as possible accessory minerals, further motivated by their grain-like appearance and dimensions of a few micrometres. Hence, the distribution of the accessory minerals in the dried structure can be identified, and porous features can be sought for in the montmorrilonite phase.

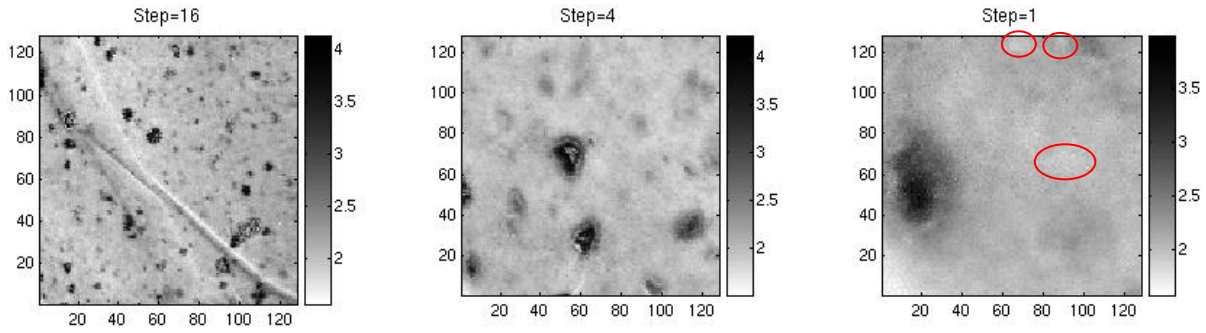

Figure 6.1. *STIM maps, 128 × 128 pixels, of a region of bentonite film on 2 µm Mylar backing. (a) 1200×1200 µm^2, (b) 300×300 µm^2 and (c) 75×75 µm^2. The lower left region in figure (a) is zoomed in in figure (b), with the same procedure between (b) and (c). Colourbars with units in mg/cm^2.*

Figure 6.2 shows a STIM map of another region, which is later also evaluated with PIXE technique (see figure 6.3). Variations in thickness can be observed, as well as more pronounced regions in the left part of the map, assumingly illustrating an assembly of accessory minerals. However, again no clear pore structure can be distinguished with confidence. It is evident that only STIM technique is not satisfactory to produce inquestionable data on the presence of pores, and the potential of the tomographic variant of STIM is presented in paragraph 6.4.

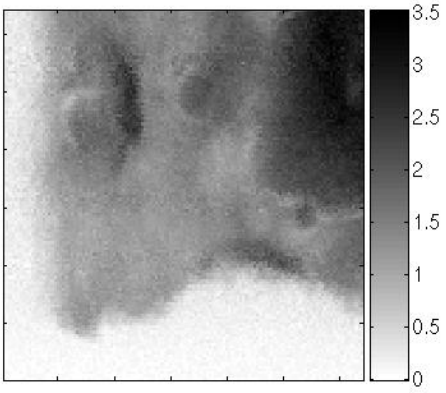

Figure 6.2. *STIM map of a corner of a bentonite film, colourbar with units in mg/cm^2, (128×128 pixels, stepsize = 0.6 μm).*

6.2 PIXE analysis

Figure 6.3 (b-f) present PIXE maps for typical bentonite components for the same sample region as in the STIM map (figure (a) and figure 6.2). Data from 4 detector elements have been added to form the element maps. Aluminium, oxygen and other elements in the montmorillonite structure, which are lighter than Z=13, can not be detected by PIXE analysis. The correlation between elements in the maps can be utilised to identify mineral phases in the sample, and distinguish accessory minerals from montmorillonite. The PIXE maps can also be used in combination with the STIM maps to identify potential pore sites. The accumulation of Fe in the lower right corner of the map is in correlation with the same region in the S map, and clearly anti-correlated with the Si map. This indicates pyrite, and this mineral grain is distinguished as a high-density spot in the STIM image. The K map indicates the presence of muscovite or K-feldspar. The spots in the Ca and Si maps could indicate the presence of a Ca-feldspar, but are not exactly correlated. Therefore, calcite is a more probable explanation for the Ca-rich region.

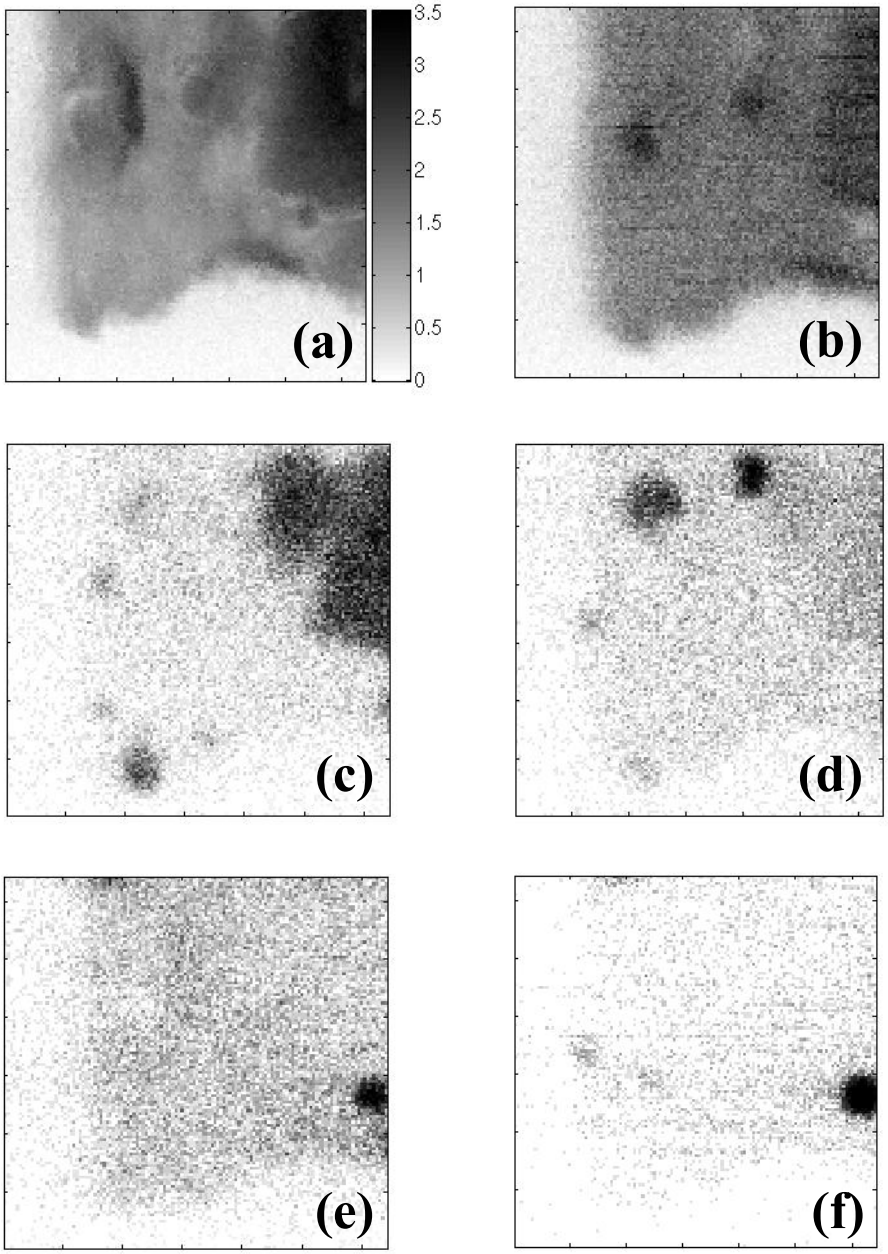

Figure 6.3. *(a) STIM map of a corner of a bentonite film, colourbar with units in mg/cm^2, (128 × 128 pixels, stepsize = 0.6 µm). Images (b)-(f) show the corresponding PIXE maps, with a slight displacement in comparison to the STIM image because of instability in the sample positioning system. (b) Si, (c) K, (d) Ca, (e) Fe, (f) S.*

6.3 Hydrogen analysis

Once hydrogen events had been identified, investigations on lateral heterogeneities were possible in a hydrogen map. Figure 6.4 (a) shows a hydrogen distribution map with the total number of hydrogen counts within an energy window set as the intensity scale. The corresponding STIM map, together with a hydrogen concentration depth profile, is presented in figure (b-c). One can observe a decrease in hydrogen events in regions that have higher mass density in the STIM map. This is in agreement with the fact that the transmitted hydrogen yield is lower for thicker samples. In regions where this correlation The hydrogen analysis showed that the sample contained approximately 0.5 wt.% hydrogen, a level of concentration that could easily be detected with the p-p scattering method. In conclusion, the hydrogen seems to be homogeneously distributed over the investigated sample region and the depth profile for an area in the right-hand side in the map, shows that the hydrogen content is fairly homogenously distributed also from the surface into the bulk down to a depth of 1 mg/cm^2. This implies that hydrogen analysis could be a favourable and useful way to investigate whether the pore number and size distribution is affected by the degree of water saturation in the clay. The hydrogen method can offer 2D hydrogen mapping with micrometer lateral resolution. In combination with depth profiling, micrometer lateral resolution is not an option for a full map, since this would require extensive irradiation times and data analysis. Therefore it is not realistic to use the hydrogen analysis alone for depth resolved direct examination of the pore structure, but rather as a complementary tool to determine the average degree of water saturation. Or, if regions of interest first are identified, scanning of smaller regions can be performed in depth profiling mode.

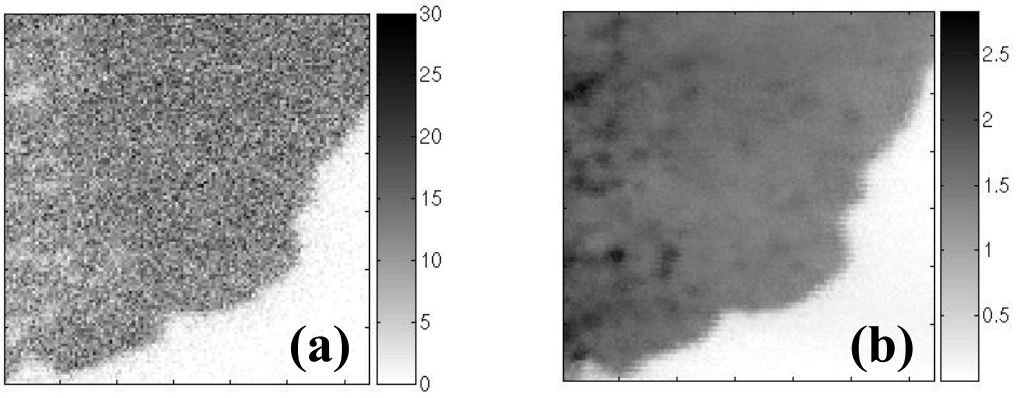

Figure 6.4. *(a) Hydrogen map (600×600 μm^2), with corresponding STIM map in (b). The colourbars show the number of hydrogen counts within an energy window and the mass density in mg/cm^2 respectively. Figure (c) shows the hydrogen depth profile (wt.% H) for an area of homogeneous thickness on the right-hand side of the sample image.*

6.4 STIM tomography

Figure 6.5 presents pictures of the tomographic reconstruction. Figure (a) shows a typical cross section (slice 20), which reveals that the mass density (g/cm^3) varies within the sample. The mass density scale ranges from blue, via turquoise to yellow and red. High-density regions can be identified (in red) and might indicate accessory minerals, and bluish and turquoise regions in central parts of the cross section indicate pores of a few micrometres in diameter. The artefacts outside the sample region are an effect of the reconstruction technique in combination with the somewhat scarce number of projections angles.

An isodensity surface is shown in figure (b) to illustrate the morphology of the bentonite strip. Here the data were smoothed and a threshold of 0.6 g/cm^3 was set as the isodensity value to be illustrated. The internal structure of the sample can be further investigated in figure (c) where 30 reconstructed cross sections have been stacked and a volume (12×12×18 µm^3) has been cut out. Although the number of projections was fewer than for an ideal reconstruction [44], a clear internal structure can be discerned, with regions of higher mass density (red colour) possibly corresponding to accessory minerals as discussed above, and regions with lower density (turquoise colour), which might indicate micrometre-sized pores.

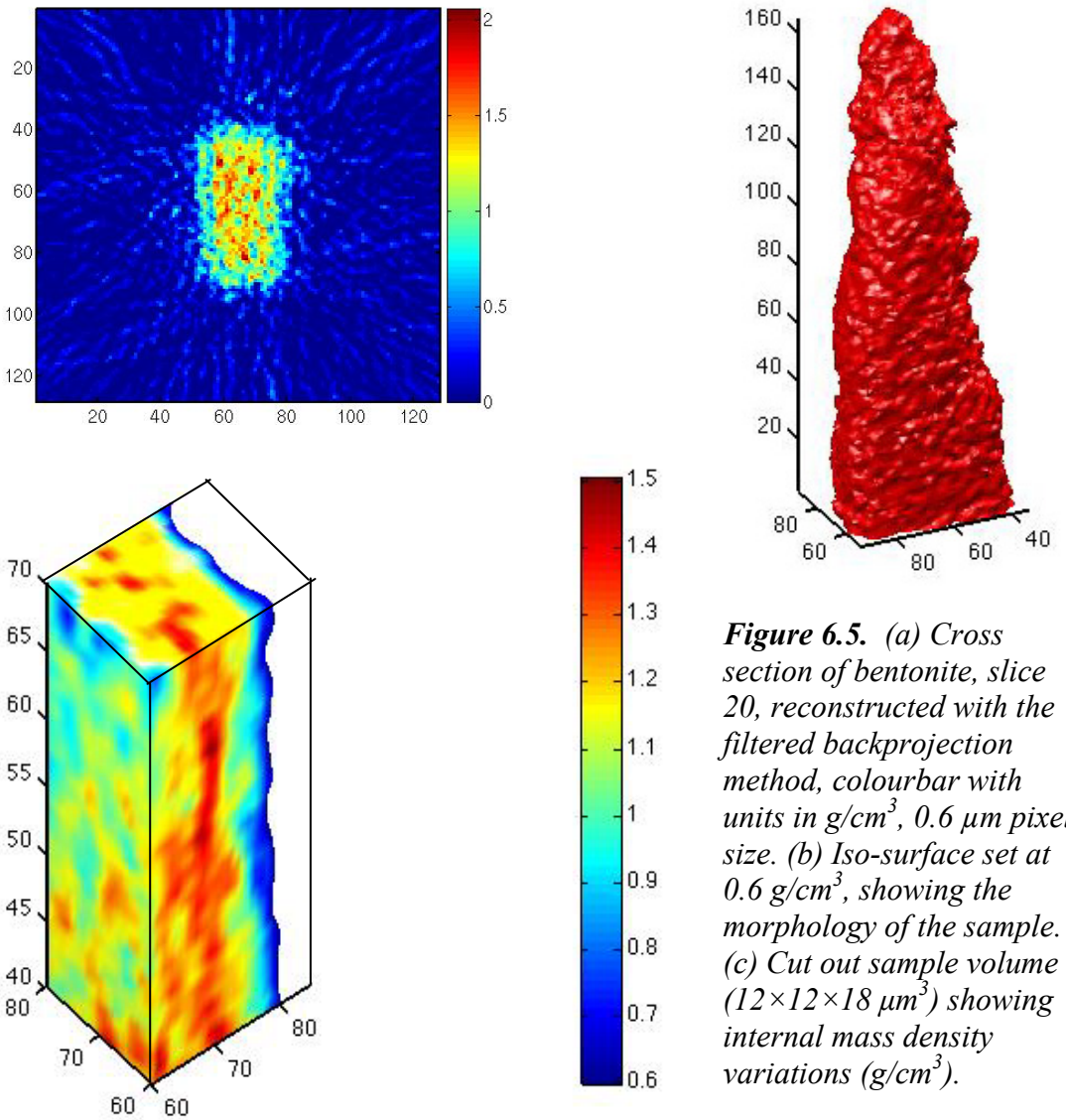

Figure 6.5. *(a) Cross section of bentonite, slice 20, reconstructed with the filtered backprojection method, colourbar with units in g/cm^3, 0.6 µm pixel size. (b) Iso-surface set at 0.6 g/cm^3, showing the morphology of the sample. (c) Cut out sample volume (12×12×18 µm^3) showing internal mass density variations (g/cm^3).*

The mass density in the pores is not zero. This can indicate that the pores are not empty or be an effect of the reconstruction technique, where data are smeared out in the backprojection process. Water-filled pores are unlikely, if considering the results of the hydrogen analysis, which stated that the material was dry. The effect of the reconstruction technique is in consistence with simulated reconstructions of noise-free phantom projection data performed with the filtered backprojection technique at the ideal number of projection angles. Small pores, with a size comparable to the pixel width, are not reconstructed as zero-density values, but the agreement between the reconstruction and the original phantom increases for larger pores. This is illustrated in figure 6.6, where a bentonite-like phantom consisting of a homogeneous base matrix stuffed with pores 1, 2 or 4 pixels in size has been reconstructed. The intensity profiles along a line through the original and reconstructed phantom do not match for zero-intensity regions, i.e. pores. It must be emphasised that proper alignment of the rotation axis is crucial for the quality and agreement of the reconstructed image, but it is also experimentally very difficult to achieve.

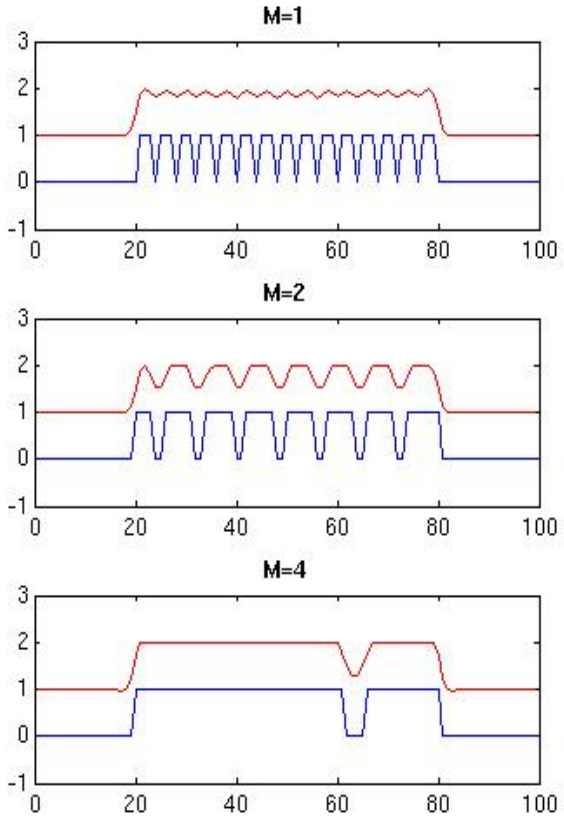

Figure 6.6. *Intensity profile from a "bentonite-like" phantom (blue) and reconstruction from simulated phantom projection data (red) with pore-sizes of 1 pixel (M=1), 2 pixels (M=2) and 4 pixels (M=4). An offset of 1 intensity unit has been applied to the reconstructed values for better visibility. Small pores are not reconstructed with the correct "zero-intensity" value. The accuracy increases with increasing simulated pore size.*

7 Summary and conclusion

Ion beam analysis has been successfully applied in the analysis of bentonite films at the Lund Nuclear Microprobe with complementary methods. STIM tomography experiments yielded information on the internal structure, and through three-dimensional mass density maps, identification of potential pores on a micrometre scale was possible. The long beam time required for the acquisition of projection data makes STIM tomography suitable for porosity studies first when regions of interest have been identified with standard two-dimensional STIM or some complementary technique.

PIXE analysis resulted in qualitative element maps, which could be used for mineral determination and identification of the porous montmorillonite phase. In combination with standard two-dimensional STIM imaging, the PIXE data can help interpreting the STIM maps and distinguish variations in sample thickness from local mass density variations. It should be emphasised that the PIXE technique within this application is useful for imaging rather than for analysis of minor and trace elements, which is the more common use. The use of PIXE for direct identification of potential sites for pores is limited, but by exploiting the spectral difference between the different elements of the 8-element HPGe detector, the technique could offer more valuable information.

Hydrogen analysis pointed out hydrogen concentrations of 0.5 wt. %, which indicates that the clay had dried so that all unbound water had been removed, probably by the high-vacuum or possibly by the ion beam. This can be compared to that during freeze drying of montmorillonite clay all but one layer of water has been shown to be removed [48]. Normally heating to 300 °C for two hours is used to remove all interlayer water [49]. However no cracks were visible in the clay plate after the measurement. This can be explained by the highly oriented nature of the sample due to the preparation method. A highly oriented clay plate will mainly contract vertically, making the sample thinner, and not horizontally which would produce cracks.

In order to continue the sample preparation technique must be further investigated and developed to ensure that the natural structure of the clay is preserved and that the water is protected from escaping during the experiment. Potential drying effects on the sample, when being introduced to the high-vacuum environment in the experiment chamber, could be investigated more in detail. This could be performed using STIM technique, with repeated measurements while pumping on the experiment chamber from atmospheric pressure down to high-vacuum.

If variations in the lateral hydrogen distribution are observed, regions of interest can possibly be analysed with depth profiling for identification and localisation of water-filled pores of micrometer size. However, the main strength of the hydrogen method is that it is a quick method for analysis of the average water content in the sample.

The survey of the feasibility of ion beam methods in the analysis of bentonite structure, has shown promising results. A future possible goal could be to perform a thorough study of samples with different water content, to investigate whether changes in porosity can be observed. STIM tomography is required for the identification of empty pores, but for water-filled pores the hydrogen method is promising. If it is proven that the sample preparation technique is capable of producing representative samples, without noticeably affecting the bentonite structure, such a study would not require a too large set of samples with varying water content to provide good pore size distribution data at the micrometer level.

References

SKB Report, R-98-10, *Systemredovisning av djupförvaring enligt KBS-3*, SKB (Swedish Nuclear Fuel and Waste Management Co), 1998.

E. Galán, *Genesis of clay minerals*, Ch. 14 Handbook of Clay Science, 2006, ISBN-13 978-0-08-044183-2.

Duane M. Moore & Robert C. Reynolds, *X-ray Diffraction and Identification and Analysis of Clay minerals*, 1997, ISBN 0-19-508713-5.

Ola Karnland & Martin Birgersson, Technical report, TR-06-11, *Montmorillonite stability*, SKB (Swedish Nuclear Fuel and Waste Management Co), 2006.

Ola Karnland, Siv Olsson, Ulf Nilsson, Technical Report, TR-06-30, *Mineralogy and sealing properties of various bentonites and smectite-rich clay minerals*, SKB (Swedish Nuclear Fuel and Waste Management Co), 2006.

A.C.D. Newman, *Chemistry of Clays and Clay minerals*, 1987, Mineral Society monograph, ISSN 0144-1485.

David A. Laird, *Influence of layer charge on swelling of smectites*, Applied Clay Science 34 (2006) 74-87.

N. Güngör, T.Tulun, A. Alemdar, Nucl. Instr. and Meth. B 142 (1998) 550-560.

Ola Karnland, Torbjörn Sandén, Lars-Erik Johannesson, Trygve E Eriksen, Mats Jansson, Susanna Wold, Karsten Pedersen, Mehrdad Motamedi, Bo Rosborg, Technical Report, TR-00-22, *Long term test of buffer materials – Final report on the pilot parcels*, SKB (Swedish Nuclear Fuel and Waste Management Co), 2000.

Ph. Ildefonse, G. Calas, A.M. Flank, P. Lagarde, Nucl. Instr. and Meth. B 97 (1995) 172-175.

S.P. Taneja and D. Raj, Nucl. Instr. and Meth. B 76 (1993) 230-232.

Luiz F. Pires, Osny O.S. Bacchi, Klaus Reichardt, Nucl. Instr. and Meth. B 229 (2005) 443-456.

Ursula Alonso, Tiziana Missana, Alessandro Patelli, Jacopo Ravagnan, Valentino Rigato, Nucl. Instr. and Meth. B 207 (2003) 195-204.

D.T. Karamanis, X.A. Aslanoglou, P.A. Assimakopoulos, N.H. Gangas, Nucl. Instr. and Meth. B 181 (2001) 616-621.

J. Miranda, A. Oliver, G. Vilaclara, R. Rico-Montiel, V.M. Macias, J.L. Ruvalcaba, M.A. Zenteno, Nucl. Instr. and Meth. B 85 (1994) 886-889.

U.A.S Tapper and K.G. Malmqvist, *Analysis, imaging, and modification of microscopic specimens with accelerator beams*, Analytical Chemistry, 1991, 63, 715 A-725 A.

A. Sakellariou, Doctoral thesis, *STIM and PIXE Tomography, The Three-Dimensional Quantitative Visualisation of Micro-Specimen Density and Composition*, University of Melbourne, 2004.

J.R. Tesmer, M. Nastasi, *Handbook of modern ion beam materials analysis*, Materials Research Society, 1995.

S.A.E. Johansson, J.L. Campbell, K.G. Malmqvist, *Particle-Induced X-ray Emission Spectrometry (PIXE)*, John Wiley and Sons Ltd, New York, 1995.

G.W. Grime, F. Watt, *Beam Optics of Quadrupole Probe-Forming Systems*, Adam Hilger, Bristol, 1994.

Kenji Kimura, Kaoro Nakajima, Hideki Imura, *Hydrogen depth profiling with sub-nm resolution in high-resolution ERD*, Nucl. Instr. and Meth. B 140 (1998) 397-401.

J. Pallon, V. Auzelyte, M. Elfman, M. Garmer, P. Kristiansson, K. Malmqvist, C. Nilsson, A. Shariff, M. Wegdén, *An off-axis STIM procedure for precise mass determination and imaging*, Nucl. Instr. and Meth. B 219-220 (2004) 988-993.

A. Shariff, Doctoral thesis, *Development of New Experimental Facilities at the Lund Nuclear Microprobe Laboratory*, Lund Institute of Technology, Lund University, 2004.

A. Shariff, K. Bülow, M. Elfman, P. Kristiansson, K. Malmqvist, J. Pallon, *Calibration of a new chamber using GUPIX software package for PIXE analysis*, Nucl. Instr. and Meth. B 189 (2002) 131-137.

Asad Shariff, Per Kristiansson, Vaida Auzelyte, Mikael Elfman, Klas G. Malmqvist, Christer Nilsson, Jan Pallon and Marie Wegdén, *Characterization of a new large area HPGe X-ray detector for low beam current application*, Nucl. Instr. and Meth. B 219-220 (2004) 494-498.

Vaida Auzelyte, Mikael Elfman, Per Kristiansson, Klas Malmqvist, Lars Wallman, Christer Nilsson, Jan Pallon, Asad Shariff and Marie Wegdén, *The beam blanking system for microlithography at Lund Nuclear Microprobe*, Nucl. Instr. and Meth. B 219-220 (2004) 485-489.

V. Auzelyte, F. Andersson, M. Elfman, P. Kristiansson, J. Pallon, M. Wegdén, C. Nilsson and N. Arteaga Marrero, *On-line measurement of proton beam current in pA range,* Nucl. Instr. and Meth. B 249 (2006) 760-763.

B.L. Cohen, C.L. Fink and J.H. Degnan, *Nondestructive Analysis for Trace Amounts of Hydrogen*, J. Appl. Phys. 43 (1972) 19.

J.F. Ziegler et. al., *Profiling hydrogen in materials using ion beams*, Nucl. Instr. and Meth. 149 (1978) 19-39.

Patrick Reichart, Doctoral thesis, *Dreidimensionale Wasserstoffmikroskopie mittels Proton-Proton Streung*, Technische Universität München, 2004.

P. Berger, J.-P. Gallien, H. Khodja, L. Daudin, M.-H. Berger and A. Sayir, *Hydrogen incorporation into high temperature protonic conductors: Nuclear microprobe microanalysis by means of $^{1}H(p,p)^{1}H$ scattering*, Nucl. Instr. and Meth. B 249 (2006) 527-531.

K. Furuno, T. Komatsubara, K. Sasa, H. Oshima, Y. Yamato, S. Ishii, H. Kimura and M. Kurosawa, *Measurement of hydrogen concentration in thick mineral or rock samples*, Nucl. Instr. and Meth. B 210 (2003) 459-463.

Bengt G. Martinsson and Per Kristiansson, *A high-sensitivity method for hydrogen analysis in thin targets*, Nucl. Instr. and Meth. B 82 (1993) 589-599.

M. Wegdén, P. Kristiansson, H. Skogby, V. Auzelyte, M. Elfman, K.G. Malmqvist, C. Nilsson, J. Pallon, A. Shariff, *Hydrogen depth profiling by p-p scattering in nominally anhydrous minerals*, Nucl. Instr. and Meth. B 231 (2005) 524-529.

Akira Ito and Hiroko Koyama-Ito, *Possible use of proton CT as a means of density normalization in the PIXE semi-microprobe analysis*, Nucl. Instr. and Meth. B 3 (1984) 584-588.

J. Huddleston, I. G. Hutchinson, T. B. Pierce and J. Foster, *Development and comparison of techniques for two-dimensional analysis using the Harwell nuclear microprope*, Nucl. Instr. and Meth. 197 (1982) 157-164.

J.F. Ziegler, SRIM 2003, Version 2003.20. Available from: http://www.srim.org

P. Formenti et al., *Heavy ion and proton beams in high resolution imaging of a fungi spore specimen using STIM tomography*, Nucl. Instr. and Meth. B 130 (1997) 230-236.

Robert MS. Schofield and Harlan W. Lefevre, *PIXE-STIM microtomography: zinc and manganese concentrations in a scorpion stinger*, Nucl. Instr. and Meth. B 72 (1992) 104-110.

G.S. Bench, A.J. Antolak, D.H. Morse, A.E. Pontau, A. Saint and G.J.F. Legge, *On the effect of beam spatial broadening in ion microtomography (IMT) image quality*, Nucl. Instr. and Meth. B 82 (1993) 447-458.

Claire Michelet, Doctoral thesis, *Développement d'une technique de micro-tomographie par faisceau d'ions a l'échelle cellulaire*, l'université Bordeaux I, 1998.

G.S. Bench and G.J.F. Legge, *High resolution STIM*, Nucl. Instr. and Meth. B 40/41 c(1989) 655-658.

A.E. Pontau, A.J. Antolak, D.H. Morse, D.L. Weirup, *Minimum data set requirements for ion microtomography*, Nucl. Instr. and Meth. B 54 (1991) 383-389.

A. Sakellariou, M. Cholewa, A. Saint and G.J.F. Legge, *An accurate reconstruction algorithm for tomography experiments that involve complex probe-sample interactions*, Meas. Sci. Technol. 8 (1997) 746-758.

Avinash C. Kak, Malcolm Slaney, *Principles of Computerized Tomo-graphic Imaging*, IEEE Press, New York, 1988, ISBN 0-87942-198-3.

Stephen G. Azevedo, Daniel J. Schneberk, J. Patrick Fitch and Harry E. Martz, *Calculation of the Rotational Centers in Computed Tomography Sinograms*, IEEE Trans. Nucl. Sci 37, nr 4, 1990.

MATLAB®, Version 7.0.4.352, MathWorks Inc., Image Processing Toolbox.

Ahlrichs, J. L., White, J. L., 1962. Freezing and lyophilizing alters the structure of bentonite gels. Science, New Series, Vol. 136, No. 3522, 1116-1118.

Brindley G. W., Brown G., 1980. Crystal structures of clay minerals and their x-ray identification. Mineralogical Society Monograph No. 5. London.